

# Deformation of C isotopes

Y. Kanada-En'yo  
*Institute of Particle and Nuclear Studies,  
High Energy Accelerator Research Organization,  
Ibaraki 305-0801, Japan*

Systematic analysis of the deformations of proton and neutron densities in even-even C isotopes was done based on the method of antisymmetrized molecular dynamics. The  $E2$  transition strength was discussed in relation to the deformation. We analyze the  $B(E2; 2_1^+ \rightarrow 0_1^+)$  in  $^{16}\text{C}$ , which has been recently measured to be abnormally small. The results suggest the difference of the deformations between proton and neutron densities in the neutron-rich C isotopes. It was found that stable proton structure in C isotopes plays an important role in the enhancement the neutron skin structure as well as in the systematics of  $B(E2)$  in the neutron-rich C.

## I. INTRODUCTION

In light unstable nuclei, exotic phenomena such as neutron halo and neutron skin structures were discovered owing to the progress of the experimental technique. These contradict to the traditional understanding for stable nuclei where the proton density and neutron densities are consistent with each other in a nucleus. These phenomena imply that the exotic features may appear in unstable nuclei due to the difference between proton and neutron densities. Another subject concerning the difference is the deformations of proton and neutron densities. For example, the opposite deformations between proton and neutron densities in proton-rich C isotopes were theoretically suggested [1].

Recently, the life time of the  $2_1^+$  state of  $^{16}\text{C}$  has been measured [2]. It indicates the abnormally small  $E2$  transition strength as  $B(E2; 2_1^+ \rightarrow 0_1^+) = 0.63 \text{ e}^2\text{fm}^4$  in  $^{16}\text{C}$ , compared with those for other C isotopes ( $^{10}\text{C}$ ,  $^{12}\text{C}$  and  $^{14}\text{C}$ ). As well known,  $B(E2)$  is related to the intrinsic deformation of the nucleus. Considering the excitation energy  $E_x(2_1^+) = 1.766 \text{ MeV}$  of  $^{16}\text{C}$ , it is expected that this nucleus is not spherical but has a deformed structure. In case of normal stable nuclei,  $B(E2)$  values are generally large in the deformed nuclei. It means that the hindrance of the  $B(E2; 2_1^+ \rightarrow 0_1^+)$  in  $^{16}\text{C}$  seems to contradict to the deformation expected from the  $E_x(2_1^+)$ . Moreover, the neutron and proton transition matrix elements,  $M_n$ ,  $M_p$  derived from the  $^{208}\text{Pb}+^{16}\text{C}$  inelastic scattering [3] imply that the neutron excitation is dominant in the  $2_1^+$  state of  $^{16}\text{C}$ . From the point of view of collective deformations, these experimental results suggest the possible difference between proton and neutron shapes in  $^{16}\text{C}$ .

In the theoretical work on the proton-rich C isotopes [1], it was suggested that the difference of the shapes between proton and neutron densities may cause the suppression of  $B(E2)$ . In the previous work [1], the difference between the proton and neutron shapes in the neutron-rich C isotopes was predicted as well as the proton-rich side. It is natural to consider that the systematic analysis of the proton and neutron deformations in connection to the  $B(E2)$  is important to understand the properties of the neutron-rich C. It may be helpful also to predict exotic phenomena in unstable nuclei.

In this paper, we study the deformations of proton and neutron densities in C isotopes based on the theoretical calculations with antisymmetrized molecular dynamics (AMD). The AMD method is a useful approach for the structure study of stable and unstable nuclei. The applicability of this method in the systematic analysis of the light nuclei has been proved in many works [4–8]. Especially, in the description of the deformation and clustering aspect in light nuclei, this method has an advantage over the normal mean-field approaches like Hartree-Fock calculations, which sometimes fail to describe the deformation in the very light nuclei such as  $^{12}\text{C}$ . Although shell model calculations are useful to investigate the level structure of light nuclei, they are not suitable for the systematic study of the deformations because of the difficulty in directly extracting intrinsic deformations as well as the ambiguity of the effective charges in the unstable nuclei. In order to extract a naive picture on the proton and neutron shapes we apply the simplest version of AMD, based on a single AMD wave function. By using the AMD method, we analyze the systematics of the deformation and  $E2$  transition strength in neutron-rich C isotopes. The hindrance of the  $E2$  transition strength in  $^{16}\text{C}$  is discussed. The theoretical predictions for the deformation and  $B(E2)$  in further neutron-rich isotopes,  $^{18}\text{C}$  and  $^{20}\text{C}$ , are also reported.

This paper is organized as follows. In section II, the formulation of AMD is briefly explained. We show the results of the energies, radii, and  $B(E2)$  obtained by the simple version of AMD, while comparing them with the experimental data in Sec.IV. In Sec.V, the intrinsic deformations of proton and neutron densities are analyzed in connection to the observable such as the  $E2$  and radii. In Sec.VI, we show the results of  $^{16}\text{C}$  obtained by an extended version of AMD. Finally, a summary is given in Sec.VII.

## II. FORMULATION

The formulation of AMD for nuclear structure studies is explained in [4,6,9].

The wave function of a system with the mass number  $A$  is written by a superposition of AMD wave functions  $\Phi_{AMD}$ . An AMD wave function is given by a single Slater determinant of Gaussian wave packets as,

$$\Phi_{AMD}(\mathbf{Z}) = \frac{1}{\sqrt{A!}} \mathcal{A}\{\varphi_1, \varphi_2, \dots, \varphi_A\}, \quad (1)$$

where the  $i$ -th single-particle wave function is written as,

$$\varphi_i = \phi_{\mathbf{x}_i} \chi_i \tau_i, \quad (2)$$

$$\phi_{\mathbf{x}_i}(\mathbf{r}_j) \propto \exp\left\{-\nu\left(\mathbf{r}_j - \frac{\mathbf{X}_i}{\sqrt{\nu}}\right)^2\right\}, \quad (3)$$

$$\chi_i = \left(\frac{1}{2} + \xi_i\right)\chi_{\uparrow} + \left(\frac{1}{2} - \xi_i\right)\chi_{\downarrow}. \quad (4)$$

In the AMD wave function, the spatial part is represented by complex variational parameters,  $X_{1i}$ ,  $X_{2i}$ ,  $X_{3i}$ , which indicate the center of the Gaussian wave packets. The orientation of the intrinsic spin is expressed by a variational complex parameter  $\xi_i$ , and the iso-spin function is fixed to be up(proton) or down(neutron).

In order to obtain a naive understanding on the systematics of intrinsic deformations, we use a simplest version of the AMD method which was applied for Li, Be and B isotopes in Ref. [4]. Namely, we perform energy variation for a parity-eigen state,  $P^{\pm}\Phi_{AMD} \equiv \Phi_{AMD}^{\pm}$ , projected from an AMD wave function. We consider the AMD wave function obtained by the energy variation as the intrinsic state, and the total-angular-momentum projection ( $P_{MK}^J$ ) is done after the variation to evaluate observables such as the energies, radii, and the transition strength. Thus the variation is done after the parity projection, but the total-angular-momentum projection is performed after the variation. This method is called as VBP (variation before projection) in the present paper. For further investigations of the level scheme of  $^{16}\text{C}$ , we also perform the VAP (variation after projection) calculation with respect to both the parity and total-angular-momentum projection as the same way as done in Refs. [9,10]. In the VBP calculations, we fix the orientation of the intrinsic spin  $\xi_i$  to be up or down. In the VAP calculations,  $\xi_i$ 's are treated as free variational parameters.

## III. INTERACTIONS

The effective nuclear interactions adopted in the present work consist of the central force, the spin-orbit force and the Coulomb force. We adopt MV1 force [11] as the central force. This central force contains a zero-range three-body force as a density-dependent term in addition to the two-body interaction. The Bertlett and Heisenberg terms are chosen to be  $b = h = 0$ . We use the parameter set, case 3 of MV1 force with the Majorana parameter as  $m = 0.576$ , which was adopted in Ref. [4]. Concerning the spin-orbit force, the same form of the two-range Gaussian as the G3RS force [12] is adopted. The strengths of the spin-orbit force, (a)  $u_I = -u_{II} \equiv u_{Is} = 900$ , and (b) 1500 MeV are used. In the VAP calculations, we also use the interaction parameters, (c) the case 1 of MV1 force with  $m = 0.62$  and the spin-orbit force with  $u_{Is} = 3000$  MeV used in Ref. [9].

## IV. RESULTS OF VBP CALCULATIONS

The structure of positive parity states of even-even C isotopes are studied by the VBP calculations within the framework of AMD. In this section, we present theoretical results, such as the energies, radii, and  $E2$  transitions, while comparing them with the experimental data. The optimum width parameter  $\nu$  in Eq.3 is chosen to minimize the energy of the system for each nucleus. The adopted  $\nu$  parameters are listed in Table.I. After the variation, we perform the total-angular-momentum projection  $P_{MK}^J$  and diagonalize the Hamiltonian and norm matrices,  $\langle P_{MK'}^J \Phi_{AMD}^{\pm} | H | P_{MK''}^J \Phi_{AMD}^{\pm} \rangle$  and  $\langle P_{MK'}^J \Phi_{AMD}^{\pm} | P_{MK''}^J \Phi_{AMD}^{\pm} \rangle$  with respect to the  $K$ -quantum ( $K', K''$ ). Consequently, we obtain  $0_1^+$  and  $2_1^+$  states which can be regarded to belong to the ground  $K^{\pi} = 0^+$  band in each C isotope. In cases of  $^{10}\text{C}$ ,  $^{16}\text{C}$  and  $^{18}\text{C}$ , the second  $2^+$  state in the  $K^{\pi} = 2^+$  band arises because of the axial asymmetry.

The binding energies and the excitation energies of the low-lying positive-parity states are shown in Fig.1 and in Table.II. The binding energies of C isotopes are systematically reproduced by the present calculations (Fig.1). As

TABLE I. The adopted width parameter  $\nu$  of the AMD wave functions for C isotopes.

	$^{10}\text{C}$	$^{12}\text{C}$	$^{14}\text{C}$	$^{16}\text{C}$	$^{18}\text{C}$	$^{20}\text{C}$
$\nu$	0.185	0.190	0.180	0.175	0.170	0.165

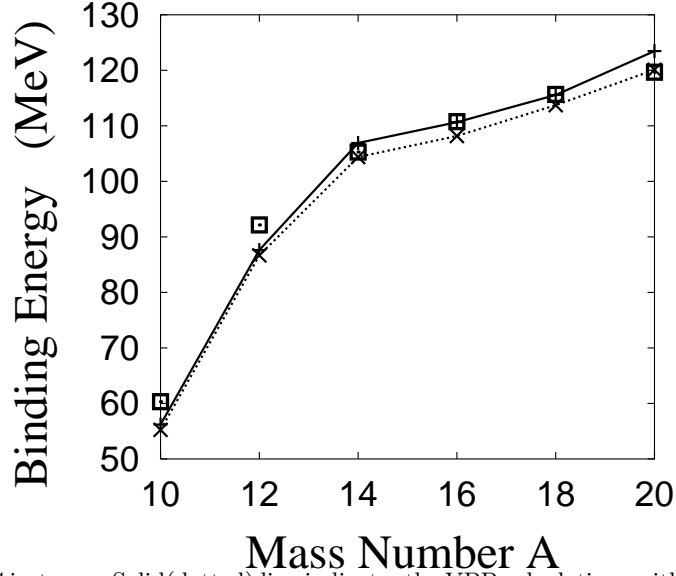


FIG. 1. Binding energies of C isotopes. Solid(dotted) line indicates the VBP calculations with  $m = 0.576$  and  $u_{ls} = 1500(900)$  MeV.

mentioned before, the second  $2^+$  state, which belong to the side band  $K^\pi = 2^+$ , is found in addition to the  $2_1^+$  state, in  $^{10}\text{C}$ ,  $^{16}\text{C}$  and  $^{18}\text{C}$ .

The excitation energies  $E_x$  of  $2_1^+$  states tend to be underestimated by the calculations, especially in the neutron-rich C isotopes. This is a general tendency of the VBP calculations where the  $0_1^+$  and  $2_1^+$  states are obtained by the total-angular-momentum projection from a single intrinsic wave function. It is considered to be because the wave function obtained in the VBP may be optimized for the  $2_1^+$  state while it is relatively not enough for the  $0_1^+$  state to reproduce the level spacing between the  $2_1^+$  and  $0_1^+$  states. In other words, the energy of  $0_1^+$  state is considered to be relatively overestimated in the VBP. The quantitative reproduction of  $E_x(2_1^+)$  is improved by VAP calculations, where the wave function is optimized for each spin-parity state. Based on the VBP and VAP calculations, the level structure of  $^{16}\text{C}$  is discussed later in Sec.VI. We give a comment that also the AMD+GCM(generator coordinate method) calculations, which is an extended version of AMD, well reproduce the  $E_x(2_1^+)$  in neutron-rich C.

Figure 2 shows the results of the root-mean-square radii comparing with the experimental radii derived from the interaction cross sections. In the systematics of the matter radii in the even-even C isotopes, there is a gap between  $^{14}\text{C}$  and  $^{16}\text{C}$ . This behavior is reproduced by the present calculations and can be described by the large deformation in  $^{16}\text{C}$  and the spherical shape due to the shell closure in  $^{14}\text{C}$ . The details are discussed in the next section.

TABLE II. Excitation energies of  $2^+$  states of C isotopes obtained by the VBP calculations.

		$^{10}\text{C}$	$^{12}\text{C}$	$^{14}\text{C}$	$^{16}\text{C}$	$^{18}\text{C}$	$^{20}\text{C}$
cal.(ls=900 MeV)	$E_x(2_1^+)$	1.80	1.45	1.69	0.40	0.61	0.57
	$E_x(2_2^+)$	2.60	—	—	1.53	0.83	—
cal.(ls=1500 MeV)	$E_x(2_1^+)$	1.95	1.66	3.75	0.65	0.87	0.88
	$E_x(2_2^+)$	3.75	—	—	2.82	1.32	—
exp.	$E_x(2_1^+)$	3.354	4.439	7.012	1.766	1.62	—
	$E_x(2_2^+)$	6.58	—	—	—	—	—

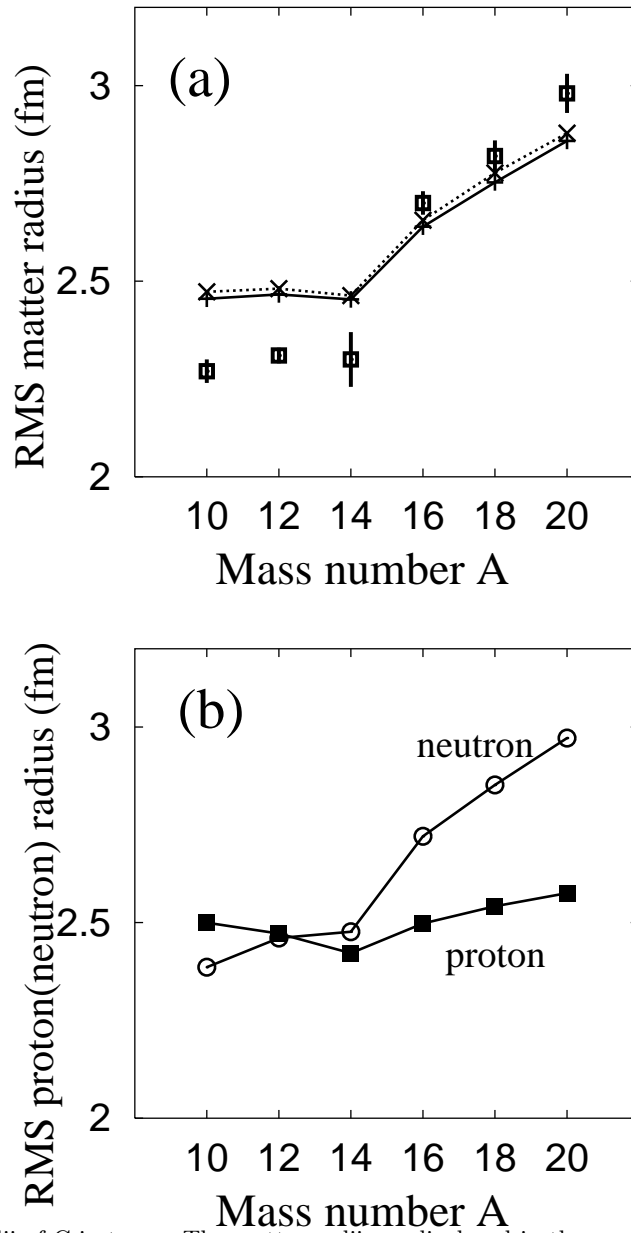


FIG. 2. Root-mean-square radii of C isotopes. The matter radii are displayed in the upper panel(a). The solid(dotted) line indicates the VBP calculations with  $m = 0.576$  and  $u_{ls} = 1500(900)$  MeV. The experimental data, which are derived from the interaction cross sections [13], are shown by cross points. The point-like proton and neutron radii calculated with  $m = 0.576$  and  $u_{ls} = 1500$  MeV are shown in the lower panel(b).

TABLE III.  $E2$  transition strength in C isotopes calculated by the VBP. The unit is  $e^2\text{fm}^4$ . The experimental data for  $^{16}\text{C}$  is taken from Ref. [2] and those for the other C are from Ref. [14].

		$^{10}\text{C}$	$^{12}\text{C}$	$^{14}\text{C}$	$^{16}\text{C}$	$^{18}\text{C}$	$^{20}\text{C}$
cal.(ls=900 MeV)	$B(E2; 2_1^+ \rightarrow 0_1^+)$	5.7	7.2	6.9	1.9	2.1	5.3
	$B(E2; 2_2^+ \rightarrow 0_1^+)$	4.3	—	—	4.7	3.8	—
cal.(ls=1500 MeV)	$B(E2; 2_1^+ \rightarrow 0_1^+)$	5.4	6.8	5.9	1.4	0.6	5.0
	$B(E2; 2_2^+ \rightarrow 0_1^+)$	3.4	—	—	4.1	4.9	—
exp.	$B(E2; 2_1^+ \rightarrow 0_1^+)$	$12.4 \pm 0.2$	$8.2 \pm 0.1$	$3.74 \pm 0.5$	0.63	—	—

The results for the  $E2$  transition strength are listed in Table.III. In the calculations, it is found that  $B(E2; 2_1^+ \rightarrow 0_1^+)$  drastically changes with the increase of neutron number in C isotopes. The theoretical  $E2$  strength in  $^{16}\text{C}$  is very small, which is consistent with the recent measurement of the abnormally small  $B(E2)$  in  $^{16}\text{C}$  [2]. The present results predict that, also in  $^{18}\text{C}$ ,  $B(E2; 2_1^+ \rightarrow 0_1^+)$  is very small as the same order of that in  $^{16}\text{C}$ . It is interesting that the calculated  $E2$  transition strength in  $^{20}\text{C}$  is not as small as those in  $^{16}\text{C}$  and  $^{18}\text{C}$ . The systematic change of the  $B(E2; 2_1^+ \rightarrow 0_1^+)$  can be understood by the deformations of proton and neutron densities in the intrinsic states as described in the next section.

## V. DISCUSSION

In this section, we analyze the intrinsic deformations of proton and neutron densities and discuss their effect on the observables such as the  $E2$  transitions and radii.

### A. intrinsic deformation

We display in Fig.3 the deformation parameters  $(\beta, \gamma)$  for the proton and neutron densities, which are defined by the moments  $\langle x^2 \rangle$ ,  $\langle y^2 \rangle$ , and  $\langle z^2 \rangle$  of the intrinsic AMD wave function as,

$$\frac{\langle x^2 \rangle^{1/2}}{(\langle x^2 \rangle \langle y^2 \rangle \langle z^2 \rangle)^{1/6}} \equiv \exp \left[ \sqrt{\frac{5}{4\pi}} \beta \cos \left( \gamma + \frac{2\pi}{3} \right) \right], \quad (5)$$

$$\frac{\langle y^2 \rangle^{1/2}}{(\langle x^2 \rangle \langle y^2 \rangle \langle z^2 \rangle)^{1/6}} \equiv \exp \left[ \sqrt{\frac{5}{4\pi}} \beta \cos \left( \gamma - \frac{2\pi}{3} \right) \right], \quad (6)$$

$$\frac{\langle z^2 \rangle^{1/2}}{(\langle x^2 \rangle \langle y^2 \rangle \langle z^2 \rangle)^{1/6}} \equiv \exp \left[ \sqrt{\frac{5}{4\pi}} \beta \cos \gamma \right]. \quad (7)$$

Here the  $x$ ,  $y$ , and  $z$  directions are chosen so as to satisfy  $\langle x^2 \rangle \leq \langle y^2 \rangle \leq \langle z^2 \rangle$  and  $\langle xy \rangle = \langle yz \rangle = \langle zx \rangle = 0$ . As seen in Fig.3, we find the drastic change of the neutron deformation in C isotopes with the increase of the neutron number. The neutron deformations are prolate, oblate and spherical in  $^{10}\text{C}$ ,  $^{12}\text{C}$  and  $^{14}\text{C}$ , respectively. In the neutron-rich region, it become prolate again in  $^{16}\text{C}$ , and they are triaxial and oblate in  $^{18}\text{C}$  and  $^{20}\text{C}$ , respectively. In contrast to the variation of neutron deformation, the proton deformations are rather stable. The deformation parameters for the proton densities lie in the oblate region  $\gamma \sim \frac{\pi}{3}$ . These behavior are the same as the results of Ref. [1].

By analysing the component of the  $K$ -quantum states ( $P_{MK}^J \Phi_{AMD}^\pm$ ) in the  $2_1^+$ , it is found that the  $2_1^+$  state can be approximately written by a single  $K = 0$  state when we chose a proper axis. Then, we can define the (approximate) principal axis  $Z$  in the body-fixed frame and form the ground  $K = 0$  band with the  $0_1^+$  and  $2_1^+$  states in each C isotope. In the systems,  $^{12}\text{C}$ ,  $^{14}\text{C}$  and  $^{20}\text{C}$ , with the oblate or spherical neutron shapes, the principal axis  $Z$  is the same as the symmetric axis  $x$  which has the smallest moment  $\langle x^2 \rangle$  as shown in Fig.4(b). In other words, the dominant component of the excited state  $2_1^+$  are the  $J_Z = K = 0$  state with respect to the symmetric axis  $x$ . It is consistent with a naive expectation for the collective rotation. It is notable that, in  $^{10}\text{C}$ ,  $^{16}\text{C}$  and  $^{18}\text{C}$ , the deformations are different between proton and neutron densities. In these nuclei, the symmetric axis for the proton shape differs from that for neutron density. Namely, the symmetric axis of the oblate proton density is the  $x$  direction, while that of the prolate neutron is the  $z$  direction. The schematic figure of the proton and neutron shapes in  $^{16}\text{C}$  is illustrated in Fig.4(a). Such the configuration of the proton and neutron shapes is energetically favored because it has the maximum overlap between the proton and neutron densities. Because of the coexistence of the different shapes between proton and neutron, the

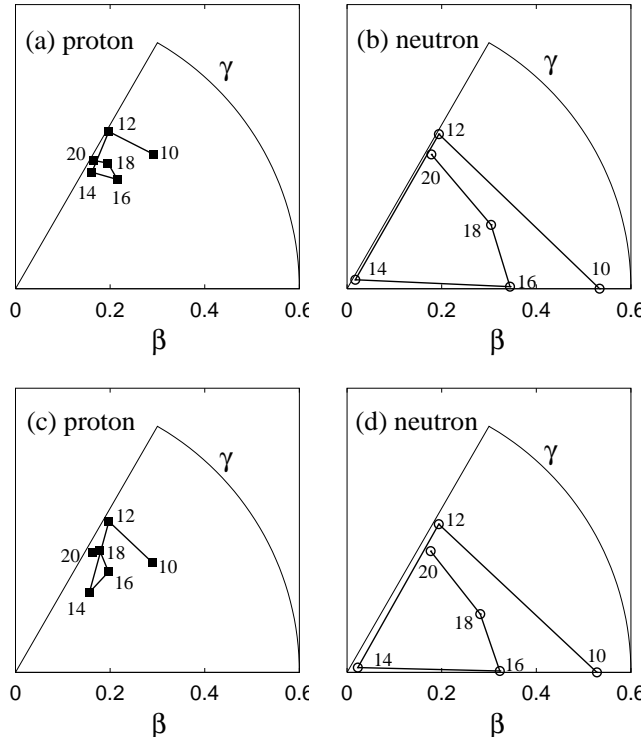


FIG. 3. Deformation parameters  $\beta, \gamma$  of the intrinsic states calculated with  $m = 0.576$ ,  $u_{ls} = 900$  MeV (a,b) and 1500 MeV (c,d). The mass numbers  $A$  are written by the corresponding points.

second  $2^+$  state appear due to the triaxiality of the total system. By analysing the component of the  $K$ -quantum states ( $P_{MK}^J \Phi_{AMD}^\pm$ ) in the excited states, it is found that the  $0_1^+$  and  $2_1^+$  states belong to the ground  $K^\pi = 0^+$  band and the  $2_2^+$  state is classified into the side-band  $K^\pi = 2^+$  when we regard the  $z$  direction with the largest moment  $\langle z^2 \rangle$  as the principal axis  $Z$  as noted in Fig.4(a). It is important that the principal axis  $Z$  is not the same as the symmetric axis  $x$  for the proton density but is perpendicular to the  $x$  in these nuclei. The existence of the side band  $K^\pi = 2^+$  in  $^{16}\text{C}$  and  $^{18}\text{C}$  has not been experimentally confirmed yet. Concerning  $^{10}\text{C}$ , the triaxiality of the mirror nucleus  $^{10}\text{Be}$  were discussed in Ref. [15], and the known  $2_2^+$  state in  $^{10}\text{Be}$  is assigned to be the band-head state of the side band  $K^\pi = 2^+$  [15,10].

We compare the matter deformation of the present results with a HF+BCS calculation with Skyrme force by Tajima et al. [16]. In the HF+BCS calculation, the C isotopes in the  $A \leq 14$  region have spherical shapes, which contradict to the knowledge that  $^{12}\text{C}$  is oblately deformed. It is natural because the mean-field calculation is considered not to be valid for very light nuclei. In the neutron-rich C, the calculated quadrupole deformation parameter is positive in  $^{16}\text{C}$  and  $^{18}\text{C}$  and oblate in  $^{20}\text{C}$  according to the HF+BCF calculation. The general behavior of the quadrupole deformation of the matter density in neutron-rich C seems to be similar with the present results, though the different shapes between proton and neutron hardly appear in the HF calculations.

## B. $E2$ transition

The intrinsic deformation is closely related to the  $E2$  transition strength. Since the present results indicate that the proton radius does not drastically change with the increase of the neutron number in C isotopes as shown in Fig.2, the  $B(E2)$  is dominantly determined by the deformations.

As mentioned before, the  $0_1^+$  and  $2_1^+$  states belong to the ground  $K^\pi = 0^+$  band, where we regard the  $x$  axis as the principal axis  $Z$  in  $^{12}\text{C}$ ,  $^{14}\text{C}$  and  $^{20}\text{C}$ , and the  $z$  axis as the  $Z$  axis in  $^{10}\text{C}$ ,  $^{16}\text{C}$  and  $^{18}\text{C}$ . In order to link the intrinsic deformations with the  $B(E2)$ , we remind the reader the well-known approximate relation between the  $B(E2)$  and the intrinsic quadrupole moment  $Q_0$ :

$$B(E2; 2_1^+ \rightarrow 0_1^+) = \frac{1}{16\pi} e^2 Q_0^2. \quad (8)$$

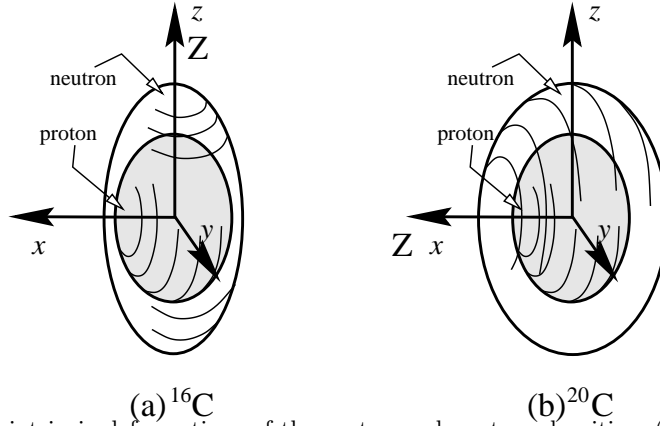


FIG. 4. Schematic figures for intrinsic deformations of the proton and neutron densities. (a) the oblate proton and prolate neutron shapes in  $^{16}\text{C}$ , and (b) the oblate proton and oblate neutron densities in  $^{20}\text{C}$ . The  $x$ ,  $y$ , and  $z$  axes are chosen to be  $\langle x^2 \rangle \leq \langle y^2 \rangle \leq \langle z^2 \rangle$ . The principal axis  $Z$  for the ground band  $J_Z = K^\pi = 0$  is also displayed.

The intrinsic quadrupole moment  $Q_0$  here is defined with respect to the principal axis as  $Q_0 = 2\langle Z^2 \rangle - \langle X^2 \rangle - \langle Y^2 \rangle$ , and is related to the deformation parameter  $\beta_p, \gamma_p$  for the proton density. In  $^{12}\text{C}$ ,  $^{14}\text{C}$  and  $^{20}\text{C}$ , where  $Z \approx x$  and  $\gamma \approx \pi/3$ ,  $Q_0$  is approximated as:

$$Q_0 = 2\langle x^2 \rangle - \langle y^2 \rangle - \langle z^2 \rangle \approx -\sqrt{\frac{5}{4\pi}} N_p e \beta_p r_e^2, \quad (9)$$

where  $N_p$  and  $r_e$  are the proton number and the root-mean-square charge radius.

In  $^{10}\text{C}$ ,  $^{16}\text{C}$  and  $^{18}\text{C}$  with  $Z \approx z$ ,  $Q_0$  depends on the deformation parameter  $\gamma_p$  as:

$$Q_0 = 2\langle z^2 \rangle - \langle x^2 \rangle - \langle y^2 \rangle \approx \sqrt{\frac{5}{4\pi}} N_p e \beta_p \cos \gamma_p r_e^2. \quad (10)$$

The important point is that the effect of the proton deformation on the  $Q_0$  decreases in these nuclei because of the factor  $\cos \gamma_p$ . Especially, in  $^{16}\text{C}$  and  $^{18}\text{C}$ , the deformation parameter  $\gamma_p \sim \pi/3$  makes the  $Q_0$  very small. This is the reason for the unusually small  $B(E2; 2_1^+ \rightarrow 0_1^+)$  in  $^{16}\text{C}$  and  $^{18}\text{C}$  shown in Table.III. In other words, the  $B(E2; 2_1^+ \rightarrow 0_1^+)$  in  $^{16}\text{C}$  and  $^{18}\text{C}$  is reduced due to the deviation the principal axis  $Z$  of the total system from the symmetric axis  $x$  for the proton density. The origin of the deviation is the different shapes between proton and neutron densities. On the other hand, it is interesting that the larger  $B(E2 : 2_1^+ \rightarrow 0_1^+)$  is predicted in  $^{20}\text{C}$ , because it has the oblate proton and neutron shapes, therefore, the principal axis aligns to the symmetric axis  $x$  as shown in Fig.4(b).

The hindrance of the  $B(E2 : 2_1^+ \rightarrow 0_1^+)$  in  $^{16}\text{C}$  can be described also from the point of view of the collective rotation. The  $2_1^+$  state of  $^{16}\text{C}$  is roughly regarded to be the state with  $J_z = K = 0$ . The  $J = 2, J_z = 0$  state is given by the linear combination of the  $J_x = 2$  state and the  $J_y = 2$  state, which are rotating around the  $x$  and  $y$  axes, respectively. The rotation around  $x$  axis causes no proton excitation, therefore, gives no contribution on the  $B(E2)$ , because  $x$  is the symmetric axis of proton density. As a result, the  $J_x = 2$  component reduces the  $B(E2 : 2_1^+ \rightarrow 0_1^+)$ . In contrast to the small  $B(E2 : 2_1^+ \rightarrow 0_1^+)$ , it is predicted that the  $B(E2 : 2_2^+ \rightarrow 0_1^+)$  in the side band is large because the  $2_2^+$  state is dominated by the  $J_z = 2$  state, where the oblate shape of the proton densities gives proton excitations.

As mentioned above, the abnormal small  $B(E2 : 2_1^+ \rightarrow 0_1^+)$  in  $^{16}\text{C}$  can be understood by the difference between oblate proton and prolate neutron shapes. Even if the proton shape in  $^{16}\text{C}$  is spherical or slightly prolate, the small  $B(E2 : 2_1^+ \rightarrow 0_1^+)$  can be also described. The characteristic of the present result is the stable proton structure in the series of C isotopes and the prediction of the second  $2^+$  state with large  $B(E2)$  in the side band. In order to conclude the intrinsic shapes of proton and neutron densities, we need further experimental information such as the systematics of  $B(E2)$  in other neutron-rich nuclei and some probes for the side-band in  $^{16}\text{C}$ .

### C. radii

In Fig.2, we present the calculated results of matter, proton and neutron radii of C isotopes while comparing them with the experimental radii which are derived from the interaction cross sections [13]. As seen in Fig.2(b), the proton

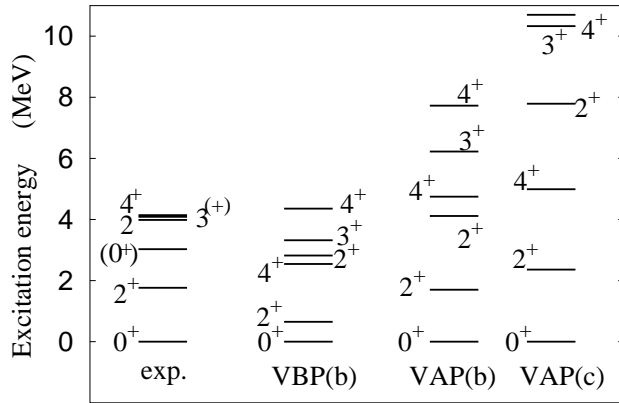


FIG. 5. Level scheme of the low-lying states of  $^{16}\text{C}$ . The theoretical results obtained by the VAP and VBP calculations with the interaction parameters (b)case 3 of MV1 with  $m = 0.576$ ,  $u_{ls} = 1500$  MeV and (c)case 1 of MV1 with  $m = 0.62$ ,  $u_{ls} = 3000$  MeV are illustrated with the experimental data.

radius does not drastically change with the increase of neutron number, while the neutron radius increases rapidly in the neutron-rich  $A \geq 16$  region. The gap of the matter radii between  $^{14}\text{C}$  and  $^{16}\text{C}$  is found to originate from a gap in neutron radii. The reason for the gap is described by the neutron deformations as follows. The neutron density is compact in  $^{14}\text{C}$  because it has a spherical shape due to the neutron shell closure. On the other hand, in  $^{16}\text{C}$ , the neutron radii is large because of the prolate deformation.

The calculated matter radii systematically reproduce the experimental data. The large matter radii in the neutron-rich region originate from the enhancement of the neutron radii. In contrast to the variation of the neutron radii, the proton radii is stable and is generally compact. As a result of the stable proton structure, the neutron skin structure enhances in the neutron-rich C isotopes. The development of neutron-skin in the C isotopes found in the present results is consistent with the results of mean-field calculations [16]. In the calculations by Thiamova et al. [8] with AMD+GCM, the radii of neutron-rich C are somehow underestimated. This is considered to be because of the lack of the three-body term in the effective force in their calculations.

## VI. RESULTS OF VAP CALCULATION

So far, we discuss the structure of C isotopes based on the VBP calculations. As mentioned before, the quantitative reproduction of the excitation energy  $E_x(2_1^+)$  in the VBP calculations is not satisfactory in the neutron-rich C. Instead, the VAP calculation [9,10] is more useful to describe the detail of the level spacing. We perform energy variation after the spin-parity projection for the  $0_1^+$ ,  $2_1^+$  and  $2_2^+$  states of  $^{16}\text{C}$ , and obtain three independent AMD wave functions. We evaluate the observables by diagonalizing the Hamiltonian and norm matrices with respect to the three wave functions as done in Refs. [9,10].

Figure 5 shows the level scheme of the low-lying states of  $^{16}\text{C}$  obtained by the VBP and VAP calculations with the interaction parameters (b) case 3 of MV1 with  $m = 0.576$ ,  $u_{ls} = 1500$  MeV. We also show the VAP results obtained by the other parameter set (c) case 1 of MV1 with  $m = 0.62$ ,  $u_{ls} = 3000$  MeV, which were adopted in Ref. [9] to reproduce well the level structure of  $^{12}\text{C}$ . The level spacing between  $0_1^+$  and  $2_1^+$  is well reproduced by the VAP calculations. The excitation energies of the side-band  $K^\pi = 2^+$  states rise comparing those with VBP. Especially, in the VAP with the interaction (c), the  $2_2^+$  state becomes relatively high because of the strong spin-orbit force.

The results of the  $E2$  transition strength in  $^{16}\text{C}$  are listed in Table.IV. Comparing the theoretical values with the experimental data, the VAP calculations tend to overestimate  $B(E2; 2_1^+ \rightarrow 0_1^+)$ . It should be noted that the triaxial shape  $\gamma_p \sim 6/\pi$  of the proton density is found in the VAP results. This is the reason for the larger  $B(E2; 2_1^+ \rightarrow 0_1^+)$  in VAP than that in VBP in which  $^{16}\text{C}$  has an oblate proton shape  $\gamma_p \sim 3/\pi$ . Because of the triaxial proton shape in VAP, the  $E2$  transition in the side band,  $B(E2; 2_2^+ \rightarrow 0_1^+)$ , is smaller than that of VBP.

In the present VAP calculations of  $^{16}\text{C}$ , the  $0_1^+$  and  $2_1^+$  level spacing is well reproduced, while the reproduction of the small  $B(E2; 2_1^+ \rightarrow 0_1^+)$  is not satisfactory. In order to insight the structure of  $^{16}\text{C}$ , we need to improve wave functions in more detail. Moreover, the further experimental information for other excited states is helpful to determine the proton shape in  $^{16}\text{C}$ .



TABLE IV. The  $E2$  transition strength in  $^{16}\text{C}$ . The theoretical results are obtained by the VAP and VBP calculations with the interaction parameters (b)  $m = 0.576$ ,  $u_{ls} = 1500\text{MeV}$  and (c)  $m = 0.62$ ,  $u_{ls} = 3000\text{MeV}$ . The unit is  $\text{e}^2\text{fm}^4$ .

	exp.	VBP(b)	VAP(b)	VAP(c)
$B(E2; 2_1^+ \rightarrow 0_1^+)$	0.63	1.4	3.7	2.7
$B(E2; 2_r^+ \rightarrow 0_1^+)$	—	4.1	2.0	2.6

## VII. SUMMARY

We studied the structure of even-even C isotopes with the AMD method. The experimental data of the binding energies,  $B(E2)$ , and radii of C isotopes are well reproduced in the present calculations. Systematic analysis of the proton and neutron shapes in C isotopes was done based on the VBP calculations of AMD. The results indicate that the neutron shape drastically changes with the increase of neutron number, while the proton shape is rather stable. It is suggested that the difference between proton and neutron shapes may appear in  $^{16}\text{C}$  and  $^{18}\text{C}$  as well as  $^{10}\text{C}$ . The  $E2$  transition strength,  $B(E2)$ , was discussed in relation to the deformation. The unusually small  $B(E2; 2_1^+ \rightarrow 0_1^+)$  in  $^{16}\text{C}$ , which has been recently measured, was described by the coexistence of the oblate proton shape and the prolate neutron shape. According to the present prediction, the  $B(E2; 2_1^+ \rightarrow 0_1^+)$  in  $^{18}\text{C}$  is as small as that in  $^{16}\text{C}$ , while the  $B(E2)$  is larger in  $^{20}\text{C}$ . The deviation between the proton and neutron shapes play an important role in the small  $B(E2)$ . The present results show the enhancement of the neutron skin structure in neutron-rich C. It was found that the stable proton structure in C isotopes plays an important role in the neutron skin structure as well as in the systematics of  $B(E2)$ .

In order to extract a naive picture on the proton and neutron shapes we applied the simplest version of AMD, based on a single AMD wave function. The quantitative reproduction of both the excitation energy ( $E_x(2_1^+)$ ) and  $B(E2)$  was not satisfactory in the present work. We consider that more detailed investigations with the improved wave functions as well as with the use of appropriate effective nuclear forces are required.

In the experiment of the  $^{208}\text{Pb}+^{16}\text{C}$  inelastic scattering, the contributions of nuclear excitation and Coulomb excitation from the ground state to the  $2_1^+(1.77\text{ MeV})$  state were analyzed [3]. The ratio of the neutron and proton transition matrix elements  $M_n/M_p$  implies the neutron excitation is dominant in the  $2_1^+$  state in  $^{16}\text{C}$ . This is consistent with the present results of oblate proton and prolate neutron shapes. Unfortunately, with this experimental information for the excitation to the  $2_1^+(1.77\text{ MeV})$ , it is difficult to know whether the proton deformation is oblate or slightly prolate (or slightly triaxial), because in both cases the sign of the  $M_p(0_1^+ \rightarrow 2_1^+)$  is same. Namely, even if the proton density has an oblate shape, the  $M_p$  is not negative but a positive value because of the different orientations of the symmetric axes between the proton and neutron shapes as shown in  $Q_0$  given by Eq.10. The characteristic of the present result is the stable proton structure and systematics of  $B(E2)$  in the series of C isotopes. If the  $^{16}\text{C}$  has the oblate proton shape, the second  $2^+$  state appears. We should stress that, whether the proton density is oblate or slightly prolate in  $^{16}\text{C}$ , the proton shape must differ from the large prolate deformation of the neutron to describe the small  $B(E2)$ . It is concluded that the small  $B(E2)$  indicates the difference between proton and neutron shapes in  $^{16}\text{C}$ . In order to understand the details of the intrinsic shapes of proton and neutron densities, we need more systematic analysis of C isotopes with the help of the further experimental information such as the  $B(E2)$  in other neutron-rich nuclei,  $^{18}\text{C}$  and  $^{20}\text{C}$ , and information for the side-band in  $^{16}\text{C}$ .

## ACKNOWLEDGMENTS

The author would like to thank Prof. H. Horiuchi, Dr. M. Takashina, and Dr. N. Itagaki for many discussions. She is also thankful to Prof. T. Motobayashi, Dr. N. Imai and Z. Elekes for valuable comments. The computational calculations in this work were supported by the Supercomputer Project Nos. 58 and 70 of High Energy Accelerator Research Organization(KEK). This work was supported by Japan Society for the Promotion of Science and a Grant-in-Aid for Scientific Research of the Japan Ministry of Education, Science and Culture. The work was partially performed in the ‘‘Research Project for Study of Unstable Nuclei from Nuclear Cluster Aspects’’ sponsored by Institute of Physical and Chemical Research (RIKEN).

## REFERENCES

---

- [1] Y.Kanada-En'yo and H.Horiuchi, Phys.Rev. C55, 2860 (1997).
- [2] N. Imai et al., Phys. Rev. Lett. **92** 062501 (2004).
- [3] Z. Elekes et al., Phys. Lett. **B 586**, 34 (2004).
- [4] Y. Kanada-En'yo, H. Horiuchi and A. Ono, Phys. Rev. C **52**, 628 (1995); Y. Kanada-En'yo and H. Horiuchi, Phys. Rev. C **52**, 647 (1995).
- [5] Y. Kanada-En'yo and H. Horiuchi, Prog. Theor. Phys. Suppl.**142**, 205(2001).
- [6] Y. Kanada-En'yo, M. Kimura and H. Horiuchi, Comptes rendus Physique Vol.4, 497(2003).
- [7] N.Itagaki and S.Aoyama, Phys.Rev. C **61**, 024303 (2000).
- [8] G.Thiamova, N.Itagaki, T.Otsuka and K.Ikeda, Nucl. Phys. **A719**, 312c (2003).
- [9] Y. Kanada-En'yo, Phys. Rev. Lett. **81**, 5291 (1998).
- [10] Y. Kanada-En'yo, H. Horiuchi and A. Doté, Phys. Rev. C **60**, 064304(1999).
- [11] T. Ando, K.Ikeda, and A. Tohsaki, Prog. Theor. Phys. **64**, 1608 (1980).
- [12] N. Yamaguchi, T. Kasahara, S. Nagata, and Y. Akaishi, Prog. Theor. Phys. **62**, 1018 (1979); R. Tamagaki, Prog. Theor. Phys. **39**, 91 (1968).
- [13] A. Ozawa et al., Nucl. Phys. **A691** 599 (2001), and references therein.
- [14] S. Raman et al., Atomic Data and Nuclear Data Tables, **36** (1987).
- [15] N.Itagaki, S.Hirose, T.Otsuka, S.Okabe and K.Ikeda, Phys.Rev. C65, 044302 (2002).
- [16] N.Tajima, S.Takahara and N.Onishi, Nucl.Phys. **A603**, 23 (1996).
- [17] N. Itagaki, S. Okabe and K. Ikeda, Phys. Rev. C **62**, 034301 (2000).